


Designing bistability or multistability in macroscopic diffusive systemsJun Wang, Gaole Dai, Fubao Yang, and Jiping Huang ^{*}*Department of Physics, State Key Laboratory of Surface Physics, and Key Laboratory of Micro and Nano Photonic Structures (MOE), Fudan University, Shanghai 200433, China*

(Received 14 September 2019; accepted 30 January 2020; published 18 February 2020)

We theoretically design a kind of diffusion bistability (and even multistability) in the macroscopic scale, which has a similar phenomenon but different underlying mechanism from its microscopic counterpart [*Phys. Rev. Lett.* **101**, 267203 (2008)]; the latter has been extensively investigated in literature, e.g., for building nanometer-scale memory components. By introducing second- and third-order nonlinear terms (that opposite in sign) into diffusion coefficient matrices, a bistable energy or mass diffusion occurs with two different steady states identified as “0” and “1.” In particular, we study heat conduction in a two-terminal three-body system and show that this bistable system exhibits a macroscale thermal memory effect with tailored nonlinear thermal conductivities. The theoretical analysis is confirmed by finite-element simulations. Also, we suggest experiments with metamaterials based on shape memory alloys. This theoretical framework blazes a trail on constructing intrinsic bistability or multistability in diffusive systems for macroscopic energy or mass management.

DOI: [10.1103/PhysRevE.101.022119](https://doi.org/10.1103/PhysRevE.101.022119)**I. INTRODUCTION**

Modern electronic techniques are facing increasingly prominent heat dissipation problems due to shrinking chip sizes and increasing integration levels [1]. Fortunately, the past decade has witnessed the possibility of manipulating heat transport at nanoscale [2–7], which provides a promising method in evolving electron-based computation. Phononics, a microscale interpretation of manipulating heat flow to carry and process information, has been flourishing since then [8]. To date, indispensable elements of phononic computers, including thermal diodes [2], thermal logical gates [3], and thermal memories [4], have been proposed theoretically and experimentally. As a basic phononic information storage, the thermal memory requests a nonlinear bistable thermal circuit, where two different steady states can be demonstrated as “0” and “1” beyond a same boundary condition, just like its electronic counterpart. Although this concept was proposed in 2008 [4], the studies of thermal bistability (TBIS) devices are still far from being satisfactory (say, compared with existing research of optical bistability), which prohibits its practical applications. A reason behind this situation is that most research is executed at microscopic scale but the nanofabrication capacity is limited.

Recent progress in TBIS focus on achieving bistable phenomenon by introducing nonlinear thermal radiation for forming the negative differential thermal resistance (NDTR) [9–15], in which the Stefan-Boltzmann law is deviated. As the success in optical bistability [16–20], it is natural to migrate its methods into thermal radiation for TBIS because both optical and thermal-radiation processes can be classified as wave physics. Comprehensively, TBIS is

realized mainly by two ways: the radiative phase transition at a specific temperature region [9–12] and the anomalous radiative phenomenon such as near-field radiation or nonlinear optical resonances [13–15]. The switching time between two states has been improved to several hundreds of microseconds in the laboratory. It seems that the nonlinear thermal radiation can be a potential theoretical scheme for achieving TBIS.

However, in a macroscopic diffusive system such as heat conduction, TBIS has never been touched because of the absence of a theoretical framework analogous to its counterpart in wave systems. Nevertheless, heat conduction, a sort of major heat-transfer mode which is described by the diffusion equation [21], cannot apply to the method in wave processes. This is because of the distinction of governing equations between diffusive and wave systems [22]. Hence, it is necessary to consider conduction TBIS due to its ubiquity. On the one hand, thermal conduction still plays a primary role of heat dissipation in traditional electron-based computation. Thermal and electronic memory may be well coupled by conduction TBIS devices. On the other hand, great progress has been made in manipulating macroscopic thermal conduction at will, especially in recent decades, by using the theory of transformation thermotics and thermal metamaterials [23–32], which may facilitate the design and manufacture of conduction TBIS devices. In this work, we establish a bistability theory for treating diffusive systems. We take heat conduction as a classical diffusive system and deduce the nonlinear-heat-conduction parameters by adopting two different theoretical methods. Finite-element simulations confirm it and further demonstrate a practical thermal memory process. We also give a proof-of-principle experimental design by adopting the temperature-trapping theory [32]. The theoretical framework applies to tailoring diffusion coefficient matrices for bistability (and multistability) in diffusive processes.

^{*}jphuang@fudan.edu.cn

II. METHOD

A diffusive system is usually described by a force causing a flux. For example, Fourier's law $\mathbf{J} = -\kappa \nabla T$ implies the heat flux is induced by a temperature gradient, similar in form to Ohm's law $\mathbf{I} = -\epsilon \nabla U$ and Fick's law $\mathbf{q} = -D \nabla n$. Generally, the relation between fluxes and forces of a diffusive system can be written as

$$Y_i = \sum_{j=1}^n K_{ij} X_j, \quad (1)$$

where i represents the variety of fluxes, and j is the symbol of different kinds of forces. Considering a simple single-field diffusion, $i = j$, Eq. (1) comes into no-coupled transport in the system. If the elements of transport coefficient tensor K_{ii} are constant, the relation between a flux Y_i and a force X_i is linear. However, bistability requests that the system deviates from a linear relation between Y_i and X_i . That is to say, nonlinearity of elements in the coefficient matrices becomes necessary for getting two or more steady-state solutions in the diffusion equation. Let us take Fourier's law as an example. Here, nonlinearity in macroscopic heat conduction can be due to the temperature dependence of thermal conductivity, $\kappa(T)$ [33]. Thus, by engineering $\kappa(T)$ of a thermal circuit, a NDTR [4,5] will work, which induces anomalous thermal diffusion. This is essentially important for obtaining macroscopic TBIS.

Inspired by the model proposed in Ref. [4], let us consider a two-terminal three-body heat transport model presented in Fig. 1(a) without loss of generality. In this case, heat flows along the x axis. A and B are two heat-conduction materials with same sizes denoted as L (length) and S (cross-sectional area). The middle small region C shows a uniform temperature distribution due to a relatively high thermal conductivity. So C is set for extracting state information of the system. We aim at observing two divergent steady temperatures within C under the same boundary condition so that TBIS is achieved. Both extremes are connected to heat baths. We fix T_h and T_c as the temperature of two heat baths, respectively, and set T_0 as the temperature of region C. According to the continuity of heat flow, T_0 has a unique solution under the steady state if A and B are linear heat-conduction materials (namely, their thermal conductivities κ_A and κ_B are temperature-independent constants). The heat flows J_A and J_B running through A and B are linear monotonic functions of T_0 , which can be verified by $J_A = \frac{\kappa_A(T_h - T_0)}{L}$ and $J_B = \frac{\kappa_B(T_0 - T_c)}{L}$. Their changes with respect to T_0 are two straight lines with one intersection point [$J_A(T_0) = J_B(T_0)$], which refers to the unique heat-conduction steady state. However, if A and B are two nonlinear-heat-conduction materials (that is, their thermal conductivities depend on temperature), the number of steady states can be increased. Here we denote $\kappa_A(T)$ and $\kappa_B(T)$ as their thermal conductivities, respectively, which can be written as

$$\kappa_A(T) = \kappa_{A0} + \sum_m \chi_{Am} T^m, \quad (2)$$

$$\kappa_B(T) = \kappa_{B0} + \sum_n \chi_{Bn} T^n, \quad (3)$$

where m and n are positive integers. The linear relation between heat flow J_A (or J_B) and T_0 is deviated. As illustrated

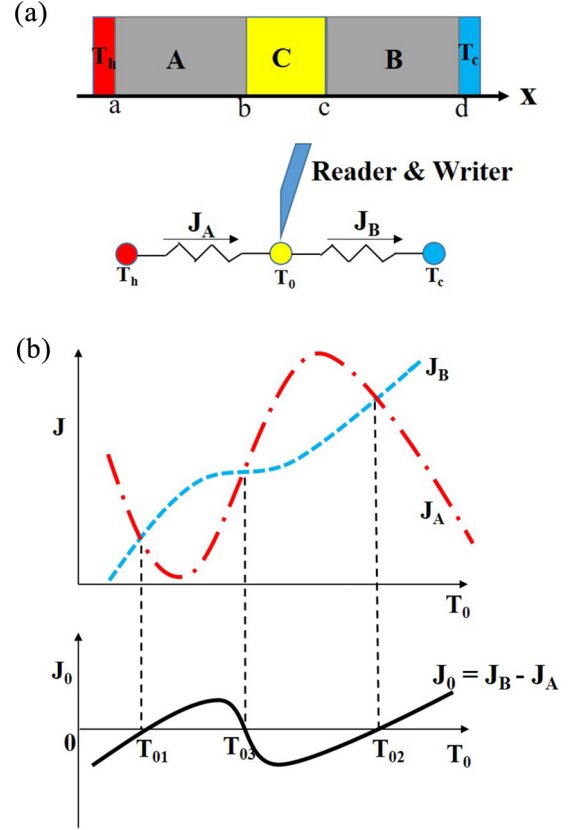


FIG. 1. (a) A two-terminal model for thermal bistability. Heat transfers along the x axis. A and B are two different heat-conduction materials. C is a region for reading out and writing in. T_h and T_c are temperatures of heat baths. T_0 is the temperature of region C. (b) Schematic diagram of heat flow in regions A (dotted red line) and B (dashed blue line), and the net flow of region C (solid black line). A and B have different nonlinear thermal conductivities, resulting in three intersections.

in Fig. 1(b), there exists more than one intersection point of J_A and J_B . That is to say, thermal bistability or multistability phenomenon can appear due to the existence of nonlinear heat conduction.

A. Calculations of net heat flow

We define $J_0 = J_B - J_A$ as the net heat flow from region C. $J_0 = 0$ is the necessary condition which a steady-state system should satisfy. In a TBIS system, $J_0(T_0) = 0$ has three real solutions. These three points are candidates of steady points. But the point of $\partial J_0 / \partial T_0 < 0$ should be excluded because it is an unstable equilibrium point. Then, which steady state will the system come into? This depends on the initial conditions. As shown in Fig. 1(b), a cubic function (rather than a quadratic function) can construct a bistable system perfectly. Thus, we can speculate that the index terms in Eqs. (2) and (3) should be kept up to the second terms. This means $m = n = 2$. Accordingly, Eqs. (2) and (3) can be reduced as

$$\kappa_A(T) = \kappa_{A0} + \chi_{A1} T + \chi_{A2} T^2, \quad (4)$$

$$\kappa_B(T) = \kappa_{B0} + \chi_{B1} T + \chi_{B2} T^2. \quad (5)$$

Distinctly, there should be two factors constraining each other in such a TBIS system. When one factor dominates, the system will come into state I (on), vice versa into state II (off). For TBIS, the dominating factors depend on the temperature-evolution direction. For example, if relaxing from a low-temperature state, factor I dominates and the system will enter state I. On the contrary, an initial high-temperature state will conclude in another final state. So χ_{A1} and χ_{A2} (or χ_{B1} and χ_{B2}) are inferred to have opposite signs. Based on the above analysis, we are in a position to calculate the thermal conductivity parameters for a TBIS system.

Under a steady state, the nonlinear-thermal-conductivity values show position dependence (one-to-one mapping to position x). But the heat flows J_A and J_B are independent of x due to heat-flow conservation. J_A can be written as

$$\kappa_{eA} = \frac{\int_{T_0}^{T_h} \kappa_A(T) dx}{T_h - T_0} = \frac{\kappa_{A0}T_h + \frac{1}{2}\chi_{A1}T_h^2 + \frac{1}{3}\chi_{A2}T_h^3 - (\kappa_{A0}T_0 + \frac{1}{2}\chi_{A1}T_0^2 + \frac{1}{3}\chi_{A2}T_0^3)}{T_h - T_0}, \quad (8)$$

$$\kappa_{eB} = \kappa_{B0}. \quad (9)$$

Substituting Eqs. (8) and (9) into Eqs. (6) and (7), we get

$$J_A = -\frac{S}{L} \left[\frac{1}{3}\chi_{A2}T_0^3 + \frac{1}{2}\chi_{A1}T_0^2 + \kappa_{A0}T_0 - \left(\frac{1}{3}\chi_{A2}T_h^3 + \frac{1}{2}\chi_{A1}T_h^2 + \kappa_{A0}T_h \right) \right], \quad (10)$$

$$J_B = \frac{S}{L} (\kappa_{B0}T_0 - \kappa_{B0}T_c). \quad (11)$$

Defining the shape factor $\Gamma = \frac{S}{L}$, then J_0 can be expressed as

$$J_0 = J_B - J_A = \Gamma \left[\frac{1}{3}\chi_{A2}T_0^3 + \frac{1}{2}\chi_{A1}T_0^2 + (\kappa_{A0} + \kappa_{B0})T_0 - \left(\frac{1}{3}\chi_{A2}T_h^3 + \frac{1}{2}\chi_{A1}T_h^2 + \kappa_{A0}T_h + \kappa_{B0}T_c \right) \right]. \quad (12)$$

Equations (4) and (5) describe the nonlinear heat conduction in the system. Generally, it is hard to solve the nonlinear-heat-conduction differential equation. So we may adopt an effective-thermal-conductivity approximation to avoid nonlinear terms in the above. In addition, the Kirchhoff transformation provides another way to make the nonlinear equation linearization [34]. As it works well in one-dimensional heat-conduction problems, we can get exact solutions of temperature distributions in our model. Then, comparing the two results, we can verify the above approximation results.

Let us still consider the nonlinear heat conduction in region A and assume region B has a linear thermal conductivity. Under a steady state, heat conduction in region A can be described as

$$\frac{\partial}{\partial x} \left[\kappa_A(T) \frac{\partial T}{\partial x} \right] = 0. \quad (13)$$

Here, we define a new variable U which has the same unit as a temperature,

$$U = U(T) = \int_{T_{\text{ref}}}^T \frac{\kappa_A(T')}{\kappa_A(T_{\text{ref}})} dT', \quad (14)$$

$J_A = \kappa_{eA}S\langle\nabla T_A\rangle$, where κ_{eA} is the effective thermal conductivity and $\langle\nabla T_A\rangle$ is the corresponding average temperature gradient of A. So is J_B . Then we can derive J_A and J_B as

$$J_A = \kappa_{eA}S\langle\nabla T_A\rangle = \frac{\kappa_{eA}(T_h - T_0)S}{L}, \quad (6)$$

$$J_B = \kappa_{eB}S\langle\nabla T_B\rangle = \frac{\kappa_{eB}(T_0 - T_c)S}{L}. \quad (7)$$

To conclude J_A and J_B , the effective thermal conductivities should be deduced. For simplicity, we assume B is a linear heat-conduction material ($\chi_{Bn} = 0$) and hold only A's nonlinearity. This simplification will not affect the cubic relation between net heat flow J_0 and T_0 . Then κ_{eA} and κ_{eB} can be written as

where T_{ref} is an arbitrary reference temperature. And Eq. (13) can be transformed as

$$\frac{\partial}{\partial x} \left[\kappa_A(T) \frac{\partial T}{\partial U} \frac{\partial U}{\partial x} \right] = 0. \quad (15)$$

Combing Eqs. (14) and (15), we can get a heat-conduction equation with U ,

$$\frac{\partial^2 U}{\partial x^2} = 0. \quad (16)$$

If we take $T_{\text{ref}} = 0$ K, the variable U and corresponding upper and lower bounds can be deduced as

$$U(T) = \frac{\int_0^T (\kappa_{A0} + \chi_{A1}T' + \chi_{A2}T'^2) dT'}{\kappa_{A0}} = \frac{\kappa_{A0}T + \frac{1}{2}\chi_{A1}T^2 + \frac{1}{3}\chi_{A2}T^3}{\kappa_{A0}}, \quad (17)$$

and

$$U_1 = \frac{\kappa_{A0}T_h + \frac{1}{2}\chi_{A1}T_h^2 + \frac{1}{3}\chi_{A2}T_h^3}{\kappa_{A0}} \quad (x = a),$$

$$U_2 = \frac{\kappa_{A0}T_0 + \frac{1}{2}\chi_{A1}T_0^2 + \frac{1}{3}\chi_{A2}T_0^3}{\kappa_{A0}} \quad (x = b). \quad (18)$$

Combing Eqs. (16) and (18) together, we can solve the expression of U as

$$U(x) = \frac{U_2 - U_1}{L}x + U_1, \quad (19)$$

which indicates the value of U at each position. It is easy to migrate $U(x)$ back to $T(x)$. Thus, by means of the

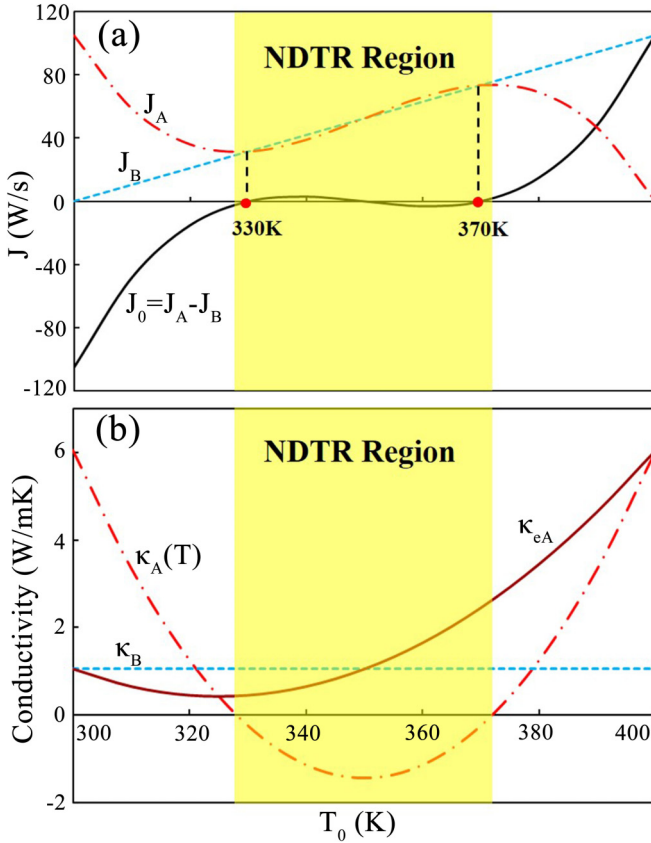


FIG. 2. Analysis of the bistability and NDTR based on the analytical model discussed in the text. (a) Heat flow in region A (dotted red line), B (dashed blue line), and net flow in region C (solid black line) vs T_0 of the system. Here B is a linear heat-conduction material and J_B curve is a straight line. J_A and J_B have three intersections. (b) Thermal conductivities of A (dotted red line) and B (dashed blue line) vs T_0 . The effective thermal conductivity of A is also shown with solid red line by integral average of T_0 . The NDTR region is shadowed in yellow, which contains two stable temperature points.

intermediate variable U , we can find the relation between T and x as

$$U = \frac{\kappa_{A0}T + \frac{1}{2}\chi_{A1}T^2 + \frac{1}{3}\chi_{A2}T^3}{\kappa_{A0}} = \frac{U_2 - U_1}{L}x + U_1. \quad (20)$$

Taking the derivative of Eq. (20) with respect to x in region A, we get $\frac{\partial T}{\partial x}|_A$,

$$\frac{\partial T}{\partial x}|_A = \frac{\kappa_{A0}(U_2 - U_1)}{\kappa_A(T)L}. \quad (21)$$

Then, the net outflow of heat from C can be written as

$$\begin{aligned} J_0^* &= J_B^* - J_A^* = \kappa_{B0} \frac{T_0 - T_c}{L} S + \kappa_A(T) \left. \frac{\partial T}{\partial x} \right|_A S \\ &= \Gamma \left[\frac{1}{3}\chi_{A2}T_0^3 + \frac{1}{2}\chi_{A1}T_0^2 + (\kappa_{A0} + \kappa_{B0})T_0 \right. \\ &\quad \left. - \left(\frac{1}{3}\chi_{A2}T_h^3 + \frac{1}{2}\chi_{A1}T_h^2 + \kappa_{A0}T_h + \kappa_{B0}T_c \right) \right], \quad (22) \end{aligned}$$

which echoes with Eq. (12). It is definite that a nonlinear one-dimensional heat-conduction process can be simplified by executing the space averaging of $\kappa(T)$, which makes a detour around the nonlinear terms. This will facilitate the disposal of the nonlinear-heat-conduction case.

B. Tailoring nonlinear-thermal-conductivities coefficients

We can see J_0 satisfies a cubic relation with T_0 . Now we construct another cubic function $J'_0(T_0)$ with three zero points T_{01} , T_{02} , T_{03} (suppose $T_c < T_{01} < T_{03} < T_{02} < T_h$). J'_0 can be written as

$$\begin{aligned} J'_0 &= \alpha[(T_0 - T_{01})(T_0 - T_{02})(T_0 - T_{03})] \\ &= \alpha[T_0^3 - (T_{01} + T_{02} + T_{03})T_0^2 \\ &\quad + (T_{01}T_{02} + T_{01}T_{03} + T_{02}T_{03})T_0 - T_{01}T_{02}T_{03}]. \quad (23) \end{aligned}$$

α is the precoefficient with a unit J/K. T_{01} and T_{02} are the two designed stable temperatures of region C. By comparing the coefficient and constant terms of Eqs. (12) and (23), we acquire a set of equations

$$\begin{aligned} \frac{1}{3}\Gamma\chi_{A2} &= \alpha, \\ \frac{1}{2}\Gamma\chi_{A1} &= -\alpha(T_{01} + T_{02} + T_{03}), \\ \Gamma(\kappa_{A0} + \kappa_{B0}) &= \alpha(T_{01}T_{02} + T_{01}T_{03} + T_{02}T_{03}), \\ -\Gamma\left(\frac{1}{3}\chi_{A2}T_h^3 + \frac{1}{2}\chi_{A1}T_h^2 + \kappa_{A0}T_h + \kappa_{B0}T_c\right) &= -\alpha T_{01}T_{02}T_{03}. \quad (24) \end{aligned}$$

Then we achieve

$$\begin{aligned} \kappa_{A0} &= \frac{\alpha}{\Gamma} \left[\frac{-T_h^3 + (T_{01} + T_{02} + T_{03})T_h^2 - (T_{01}T_{02} + T_{01}T_{03} + T_{02}T_{03})T_c + T_{01}T_{02}T_{03}}{T_h - T_c} \right], \\ \kappa_{B0} &= \frac{\alpha}{\Gamma} \left[\frac{T_h^3 - (T_{01} + T_{02} + T_{03})T_h^2 + (T_{01}T_{02} + T_{01}T_{03} + T_{02}T_{03})T_h - T_{01}T_{02}T_{03}}{T_h - T_c} \right], \\ \chi_{A1} &= -\frac{2\alpha}{\Gamma}(T_{01} + T_{02} + T_{03}), \\ \chi_{A2} &= \frac{3\alpha}{\Gamma}. \quad (25) \end{aligned}$$

We can see χ_{A1} and χ_{A2} have opposite signs definitely, which echo with the inference above. In fact, this is a feature of a bistable system with two kinds of factors competing in the process of evolution from a nonequilibrium state to an equilibrium state. T_{01} and T_{02} are representations of two different states, while T_{03} cannot exist in a steady state. Equation (25) provides guidance in designing nonlinear parameters of heat-conduction objects to realize TBIS. We can calculate the coefficients according to the preset zero-point temperatures (T_{01} , T_{02} , and T_{03}), the temperatures of heat baths, and two factors Γ and α .

According to this method, a diffusive system can indeed exhibit bistable states by engineering nonlinear transport coefficients. This intrinsic bistability depends on two competitive factors, which are reflected by two nonlinear terms with opposite signs. We prove that the second- and third-order nonlinearity of transport coefficients makes bistability effects valid. If the nonlinearity orders are higher, multistability can come to appear. And the switching time depends on the diffusion velocity of heat or mass.

III. NUMERICAL ANALYSIS AND SIMULATION

We draw the graphs to illustrate our methods for tailoring nonlinear thermal conductivities. On basis of the model shown in Fig. 1(a), we set $T_{01} = 330$ K, $T_{02} = 370$ K, and $T_{03} = 350$ K. The heat and cold baths are fixed at 400 and 300 K, respectively. Two factors are set as $\alpha = 0.001$ J/K and $\Gamma = 1$ m. The substitution of these parameters into Eq. (25) yields $\kappa_{A0} = 366.05$ J/(mK), $\kappa_{B0} = 1.05$ J/(mK), $\chi_{A1} = -2.1$ J/(mK²), and $\chi_{A2} = 0.003$ J/(mK³). The curves of J_A , J_B , and J_0 vs T_0 are shown in Fig. 2(a). Three intersections emerge, corresponding to the preset parameters T_{01} , T_{02} , and T_{03} . In Fig. 2(b), the thermal conductivities of A and B vs temperature are depicted. We can see $\kappa_A(T)$ has negative values in a certain temperature region. This is calculated as (328.02 K, 371.98 K), which refers to the NDTR region (see yellow-shadowed region in Fig. 2). The region completely contains two stable temperatures, confirming that the desired TBIS is induced by the NDTR. These two graphs accord with our expected results, as sketched in Fig. 1(b).

When the coefficients of nonlinear thermal conductivities have slight variations, will TBIS be broken? Here, we give a 1% value shift to four parameters (κ_{A0} , κ_{B0} , χ_{A1} , and χ_{A2} are increased by 1%, respectively). According to the comparisons in Fig. 3, the small shift of κ_{B0} cannot affect the TBIS. This can be interpreted that the steady heat flow in the system stays almost unchanged. While the thermal conductivity of A varies slightly, TBIS will not exist anymore. So we can conclude that the TBIS of heat conduction is parameter sensitive. This strict limitation makes it hard to observe the TBIS phenomenon in practical heat-conduction materials. But we can carefully tailor an intrinsic TBIS with predesigned zero-point temperatures.

We perform finite-element simulations based on the commercial software COMSOL MULTIPHYSICS [35]. We build a model with 9 cm length and 1 cm width. Heat conducts along the x axis. The thermostat region is placed in the

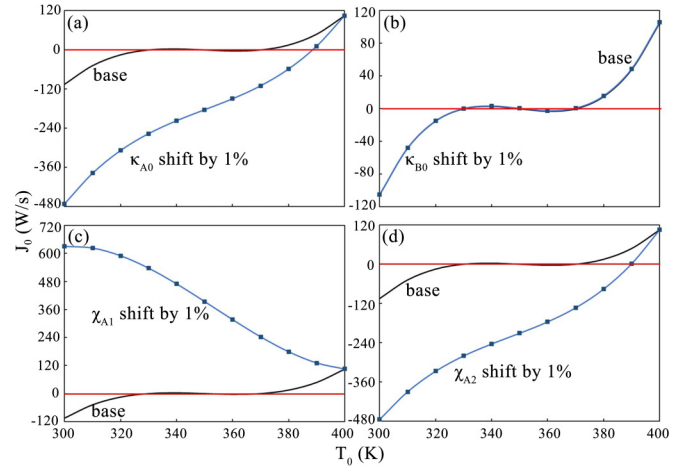


FIG. 3. Net flow J_0 vs T_0 for different small-shift coefficients. (a) TBIS behavior for different linear coefficients κ_{A0} . (b) TBIS behavior for different linear coefficients κ_{B0} . (c) TBIS behavior for different second-order coefficients χ_{A1} . (d) TBIS behavior for different third-order coefficients χ_{A2} .

central region with $\kappa_C = 1000$ J/(mK). For the thermal conductivities of left and right parts, we give 400, 500, and 600 K as three predesigned zero points. Γ is $\frac{1}{4}$ m according to the model's geometry. α is arbitrary, and here we take it as 0.0001 J/K. Thus, we can calculate that $\kappa_{A0} = 290$ J/(mK), $\kappa_{B0} = 6$ J/(mK), $\chi_{A1} = -1.2$ J/(mK²), and $\chi_{A2} = 0.0012$ J/(mK³). The density and specific heat of all materials are set as 10 kg/m³ and 10 J/(kg K). Boundary conditions are fixed at 700 (left) and 300 K (right). Then, we give 300 and 700 K, respectively, as initial surface temperatures, see Fig. 4(a). After the temperature evolution within 0.004 s, the system comes into stable states. However, the final temperatures of C are different according to different initial temperatures, which represent two different stable states. The initial temperature 300 K induces 398.46 K (stable state I) in C, while 700 K leads to 600.12 K (stable state II). The states of C depend on the initial surface temperatures. We fetch the final-state-temperature data of the model along the x axis and curve it in Fig. 4(b). States I and II have two different platform temperatures in region C (4~5 cm), as expected. In addition, we plot the theoretical results of heat flow and thermal conductivities versus T_0 as inset diagrams in Fig. 4(b). Both 400 and 600 K are the preset stable values for designing the thermal conductivity parameters. And the simulation results confirm the theoretical values very well.

Then we demonstrate an overall thermal memory process with the designed conduction TBIS in Fig. 5(a), which is based on the simulation results in the above. First, we initialize the model by a temperature writer in 300 K as an initial temperature. After 0.004 s, the system will come into steady state, and we read out T_0 in region C by a temperature reader. It is 398.46 K now. And then we write in another temperature as 700 K. After 0.004 s, a steady temperature of 600.12 K can be read out. In this model, the switching time is 0.004 s, which depends on the density and specific heat of each part. So these two parameters should be taken

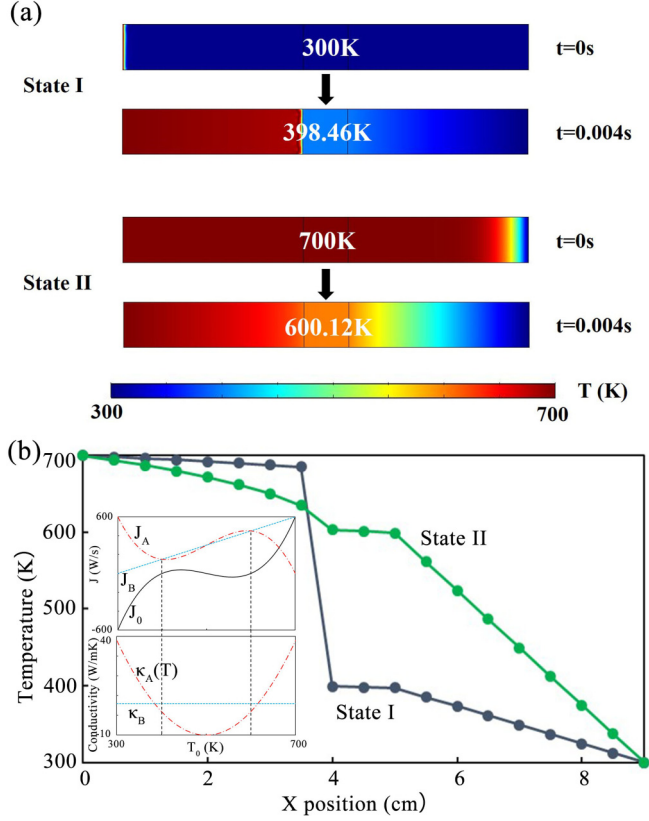


FIG. 4. Finite-element simulations of TBIS. (a) Transient simulation results beyond fixed heat bath temperatures. After 0.004 s, the system comes into a stable state with two different T_0 values due to the different initial temperatures. (b) Temperature distribution along the x axis. The left end of the model is set as the origin point ($x = 0$). Theoretical heat flows and thermal conductivities of the model are shown for comparison with the simulation results in vignettes.

into consideration and optimized when devices are in practical application. This memory process makes the conduction TBIS practical in fabricating macroscopic thermal memory components.

IV. EXPERIMENTAL DESIGN

The temperature-trapping theory [32] inspires us to design a proof-of-principle experiment. This theory implies a thermostat region in the center of a spatially symmetric structure within shape memory alloys (SMAs). The thermostat's temperature depends entirely on the critical temperature of SMAs. Here, we improve this structure and design a two-stage-SMAs device to achieve TBIS, as shown in Fig. 5(b). Two pairs of SMAs are arrayed at both sides, which are in white and gray, respectively, forming two-stage thermal switches. Different types of SMAs are applied in each pair. In particular, these two stages have different critical temperatures T_1 and T_2 , where $T_1 < T_2$. In detail, the white stage on the left levels below T_1 and bends above T_1 , while the right one shows the same T_1 but inverse deformation. The similar rule works on the gray stage. Heat and cold baths are fixed on both sides with $T_h > T_2$ and $T_c < T_1$. When the whole device is initialized under a low temperature in the left part and a high temperature in right, all

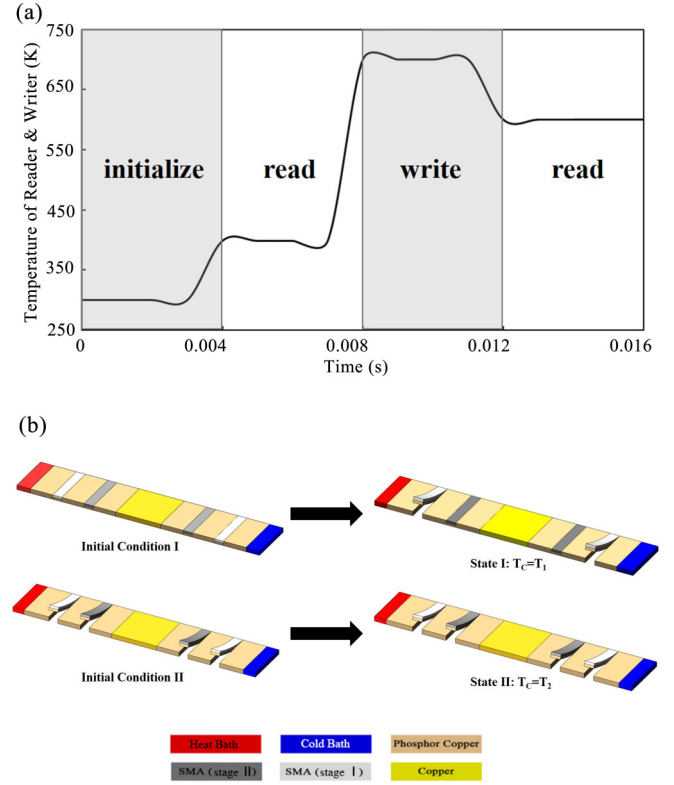


FIG. 5. (a) A demonstration of thermal memory process with the model we design. Four stages are displayed as initialization, reading-out, writing-in, and reading-out. (b) An experimental design based on the temperature-trapping theory. Two stages with different types of SMA are arrayed. The central temperatures depend on the SMA-stages' critical temperatures.

the SMAs get straight. When coming to the steady state, the outer stage bends and the heat flow cannot run into the inner layer. The thermostat's temperature approaches T_1 . When the initial condition reverses, all stages bend. They will not be level at steady state as $T_h > T_2$ and $T_c < T_1$. This process induces another steady state that T_2 is the final temperature of the thermostat. As the SMAs are commercially available, it is feasible to assemble such a two-stage structure. But the thermal contact resistances may affect the experimental results, which should be considered further.

V. DISCUSSION AND CONCLUSION

For the temperature-dependent thermal conductivity of A depicted in Fig. 1(a), the third-order nonlinearity is just a necessary condition. We can find that $|\kappa_{A0}| \sim |\chi_{A1}T| \sim |\chi_{A2}T^2|$ is another parameter requirement. Fortunately, these extraordinary thermal properties were proved to emerge in some bulk nonmetallic solids [36]. For example, the thermal conductivity of bulk ZrO_2 is $4.00 - 8.72 \times 10^{-3}T + 1.28 \times 10^{-5}T^2 - 5.82 \times 10^{-9}T^3$ [W/(m K)], which agrees qualitatively with the conduction TBIS requires at the 10^3 -K level. It can be applied as material A in our model, combining with a common material B. By solving the inverse solutions of Eq. (24), namely, working out α , T_{01} , T_{02} , and T_{03} , one can estimate the experimental bistable temperature for such

a structure composed of a nonlinear bulk heat-conduction material plus a common material. Thus, the observation of conduction TBIS in natural materials is practically probable. Besides, by means of the composite effect of nonlinear heat transfer [37], the fabrication of a conduction TBIS device with composite materials is possible. In this case, the nonlinear thermal conductivities can be well tailored if adjusting the fraction or configuration of the composite bulk's components [38]. For example, a core-shell structure [33] and a particle-embedded-in-host structure [39] may be candidates. So we also suggest the composite manufacture method as material A in fabricating the device for application scenarios.

Heretofore, we have established a theoretical framework for achieving bistability in heat diffusive systems. We prove that the TBIS phenomenon exists not only in the wave process (say, nonlinear thermal radiation) but also can be realized in heat-conduction systems. Second- and third-order nonlinearity of thermal conductivity can induce a bistable thermal circuit. When the nonlinearity orders go higher, multistability can be observed as well. We have also given numerical calculation results and show that the TBIS in heat conduction is parameter sensitive. Besides, a completed thermal memory process is demonstrated with four stages as an evident consequence. Except for thermal memories, ther-

mal switch is another possible application. As the designed experiment implies, the switch is initial-temperature forced and can barrier or allow heat flows due to distinguishable thermal conductivities. As waste heat is dissipated mainly by the diffusive process in traditional computers, conduction TBIS devices can thus be coupled with electronic devices, which facilitates thermal calculation based on existing electric calculation.

In summary, we introduce an approach of designing macroscopic bistability by taking the heat-conduction process as a typical case. Due to the form or similarity of the governing equations, this method is applicative in arbitrary diffusive systems, for example, in DC systems or particle-diffusion systems. By tailoring spatial asymmetry and nonlinearity of diffusive parameters carefully, the bistability or multistability can be realized. This method not only helps generate a significant physical phenomenon in macroscopic diffusive processes but also serves as a potential tool in macroscopic energy or mass management.

ACKNOWLEDGMENT

We acknowledge financial support by the National Natural Science Foundation of China under Grant No. 11725521.

-
- [1] M. Maldovan, Sound and heat revolutions in phononics, *Nature (London)* **503**, 209 (2013).
 - [2] B. Li, L. Wang, and G. Casati, Thermal Diode: Rectification of Heat Flux, *Phys. Rev. Lett.* **93**, 184301 (2004).
 - [3] L. Wang and B. Li, Thermal Logic Gates: Computation with Phonons, *Phys. Rev. Lett.* **99**, 177208 (2007).
 - [4] L. Wang and B. Li, Thermal Memory: A Storage of Phononic Information, *Phys. Rev. Lett.* **101**, 267203 (2008).
 - [5] W. Lee, K. Kim, W. Jeong, L. A. Zotti, F. Pauly, J. C. Cuevas, and P. Reddy, Heat dissipation in atomic-scale junctions, *Nature (London)* **498**, 209 (2013).
 - [6] K. C. Balram, M. I. Davanco, J. D. Song, and K. Srinivasan, Coherent coupling between radiofrequency, optical and acoustic waves in piezo-optomechanical circuits, *Nat. Photonics* **10**, 346 (2016).
 - [7] J. Lee, W. Lee, G. Wehmeyer, S. Dhuey, D. L. Olynick, S. Cabrini, C. Dames, J. J. Urban, and P. Yang, Investigation of phonon coherence and backscattering using silicon nanomeshes, *Nat. Commun.* **8**, 14054 (2017).
 - [8] N. Li, J. Ren, L. Wang, G. Zhang, P. Hanggi, and B. Li, Colloquium: Phononics: Manipulating heat flow with electronic analogs and beyond, *Rev. Mod. Phys.* **84**, 1045 (2012).
 - [9] R. Xie, C. T. Bui, B. Varghese, Q. Zhang, C. H. Sow, B. Li, and J. T. L. Thong, An electrically tuned solid-state thermal memory based on metal-insulator transition of single-crystalline VO₂ nanobeams, *Adv. Funct. Mater.* **21**, 1602 (2011).
 - [10] C. Wu, F. Feng, and Y. Xie, Design of vanadium oxide structures with controllable electrical properties for energy applications, *Chem. Soc. Rev.* **42**, 5157 (2013).
 - [11] P. Ben-Abdallah and S. Biehs, Near-Field Thermal Transistor, *Phys. Rev. Lett.* **112**, 044301 (2014).
 - [12] V. Kublytskyi, P. Ben-Abdallah and S. Biehs, Radiative Bistability and Thermal Memory, *Phys. Rev. Lett.* **113**, 074301 (2014).
 - [13] M. Elzouka and S. Ndao, Near-field nanothermomechanical memory, *Appl. Phys. Lett.* **105**, 243510 (2014).
 - [14] C. Khandekar and A. W. Rodriguez, Thermal bistability through coupled photonic resonances, *Appl. Phys. Lett.* **111**, 083104 (2017).
 - [15] A. M. Morsy, R. Biswas, and M. L. Povinelli, High temperature, experimental thermal memory based on optical resonances in photonic crystal slabs, *APL Photonics* **4**, 010804 (2019).
 - [16] D. J. Bergman, O. Levy, and D. Stroud, Theory of optical bistability in a weakly nonlinear composite medium, *Phys. Rev. B* **49**, 129 (1994).
 - [17] L. Gao, L. Gu, and Z. Li, Optical bistability and tristability in nonlinear metal/dielectric composite media of nonspherical particles, *Phys. Rev. E* **68**, 066601 (2003).
 - [18] N. M. Litchinitser, I. R. Gabitov, and A. I. Maimistov, Optical Bistability in a Nonlinear Optical Coupler with a Negative Index Channel, *Phys. Rev. Lett.* **99**, 113902 (2007).
 - [19] P. Y. Chen, M. Farhat, and A. Alù, Bistable and Self-Tunable Negative-Index Metamaterial at Optical Frequencies, *Phys. Rev. Lett.* **106**, 105503 (2011).
 - [20] Y. Huang and L. Gao, Tunable Fano resonances and enhanced optical bistability in composites of coated cylinders due to nonlocality, *Phys. Rev. B* **93**, 235439 (2016).
 - [21] T. N. Narasimhan, Fourier's heat conduction equation: History, influence, and connections, *Rev. Geophys.* **37**, 151 (1999).
 - [22] K. V. Zhukovsky and H. M. Srivastava, Analytical solutions for heat diffusion beyond Fourier law, *Appl. Math. Comp.* **293**, 423 (2017).

- [23] C. Z. Fan, Y. Gao, and J. P. Huang, Shaped graded materials with an apparent negative thermal conductivity, *Appl. Phys. Lett.* **92**, 251907 (2008).
- [24] T. Y. Chen, C.-N. Weng, and J.-S. Chen, Cloak for curvilinearly anisotropic media in conduction, *Appl. Phys. Lett.* **93**, 114103 (2008).
- [25] S. Guenneau, C. Amra, and D. Veynante, Transformation thermodynamics: Cloaking and concentrating heat flux, *Opt. Express* **20**, 8207 (2012).
- [26] S. Narayana and Y. Sato, Heat Flux Manipulation with Engineered Thermal Materials, *Phys. Rev. Lett.* **108**, 214303 (2012).
- [27] R. Schittny, M. Kadic, S. Guenneau, and M. Wegener, Experiments on Transformation Thermodynamics: Molding the Flow of Heat, *Phys. Rev. Lett.* **110**, 195901 (2013).
- [28] H. Y. Xu, X. H. Shi, F. Gao, H. D. Sun, and B. L. Zhang, Ultrathin Three-Dimensional Thermal Cloak, *Phys. Rev. Lett.* **112**, 054301 (2014).
- [29] T. C. Han, X. Bai, D. L. Gao, J. T. L. Thong, B. W. Li, and C.-W. Qiu, Experimental Demonstration of a Bilayer Thermal Cloak, *Phys. Rev. Lett.* **112**, 054302 (2014).
- [30] Y. G. Ma, Y. C. Liu, M. Raza, Y. D. Wang, and S. L. He, Experimental Demonstration of a Multiphysics Cloak: Manipulating Heat Flux and Electric Current Simultaneously, *Phys. Rev. Lett.* **113**, 205501 (2014).
- [31] Y. Li, X. Y. Shen, Z. H. Wu, J. Y. Huang, Y. X. Chen, Y. S. Ni, and J. P. Huang, Temperature-Dependent Transformation Thermotics: From Switchable Thermal Cloaks to Macroscopic Thermal Diodes, *Phys. Rev. Lett.* **115**, 195503 (2015).
- [32] X. Y. Shen, Y. Li, C. R. Jiang, and J. P. Huang, Temperature Trapping: Energy-Free Maintenance of Constant Temperatures as Ambient Temperature Gradients Change, *Phys. Rev. Lett.* **117**, 055501 (2016).
- [33] S. Yang, L. J. Xu, and J. P. Huang, Metathermotics: Nonlinear thermal responses of core-shell metamaterials, *Phys. Rev. E* **99**, 042144 (2019).
- [34] W. Nakwaski, Static thermal properties of broad-contact double-heterostructure laser diodes, *Opt. Quantum Electron.* **15**, 513 (1983).
- [35] <http://www.comsol.com/>.
- [36] Y. S. Touloukian, P. E. Livey, and S. C. Saxena, *Thermal Conductivity: Nonmetallic Solids* (IFI/Plenum Press, New York, 1970).
- [37] G. Lu, X. D. Wang, Y. Y. Duan, and X. W. Li, Effects of non-ideal structures and high temperatures on the insulation properties of aerogel-based composite materials, *J. Non-Cryst. Solids* **357**, 3822 (2011).
- [38] Y. J. Dai, Y. Q. Tang, W. Z. Fang, H. Zhang, and W. Q. Tao, A theoretical model for the effective thermal conductivity of silica aerogel composites, *Appl. Therm. Engin.* **128**, 1634 (2018).
- [39] G. L. Dai, J. Shang, R. Z. Wang and J. P. Huang, Nonlinear thermotics: Nonlinearity enhancement and harmonic generation in thermal metasurfaces, *Eur. Phys. J. B* **91**, 59 (2018).